The influence of bath temperature on the one-step electrodeposition of non-wetting copper oxide coatings

Raziyeh Akbari, Guilhem Godeau, Mohammadreza Mohammadizadeh, Frédéric Guittard, Thierry Darmanin

The influence of bath temperature on the one-step electrodeposition of non- wetting copper oxide coatings

Raziyeh Akbari[1, 2], Guilhem Godeau[2], Mohammadreza Mohammadizadeh[1], Frédéric Guittard[2], & Thierry Darmanin[*,2]

[1] Supermaterials Research Lab (SRL), Department of Physics, University of Tehran, North Kargar Av., 14395-547, Tehran, Iran

[2] Université Côte d'Azur, NICE Lab, IMREDD, 06200 Nice, France

* Thierry.DARMANIN@univ-cotedazur.fr

Abstract

Currently, the use of smart surfaces in the industries is well developed due to enhanced durability and qualification of fabricated layers as well as the increased values of products. Herein, the hydrophobic copper and cuprite surfaces were fabricated via the electrodeposition at various bath temperatures ranging from 15 to 90 °C by galvanostatic and cyclic voltammetry approaches. The layers were grown in the Cu_2O (111) and Cu (002) directions in the galvanostatic and cyclic voltammetry methods, respectively which are in agreement with the SEM images of surface crystals. In fact, in the galvanostatic samples, triangles and octahedral pyramids were formed in the size of 100 to 600 nm while the 1 to 6 µm crystals with flat facets were formed using the cyclic voltammetry. In general, the size and swelling of the crystals are increased by raising the bath temperature. Actually, the higher hydrophobicity was observed in the prepared sample at 75 °C using cyclic voltammetry where the water droplet adhered to the surface (parahydrophobic) with a large contact angle (θ_W = 147º). This sample was also converted to superhydrophobic with a small sliding angle (θ_{SA} < 3º) after one year rest in a sealed glass box.

Keywords: Nanostructure, Wetting, Electrodeposition, Copper, Bath temperature.

PACS: 68.08.Bc, 71.20.-b, 68.08.-p, 81.15.Pq.

1. Introduction

Recently, engineering of smart and advanced functional coatings has attracted extensive attention in the real applications in marine, automobile and environmental used tools [1,2]. In addition, the durability and advances of these smart technological surfaces would be increased significantly by including the water-repellent property of hydrophobic layers resulting enhancement of the applications in the self-cleaning, anti-icing, anti-fouling and drag reduction properties [3,4]. These surfaces are generally classified according to the water contact and sliding angle on them (θ_W and θ_{SA}, respectively). In fact, a non-wetting surface with high θ_W and θ_{SA} is called parahydrophobic and it is titled superhydrophobic having high θ_W and low θ_{SA} [5-9]. The water droplet detaches from the surface easily in the latest case. According to the experimental findings, fabrication of the non-wetting surfaces is reachable by combining the low surface energy materials with the art of fabrication of special surface patterns. This may enhance the amount of the trapped air pockets inside the roughness of surface [9-11], which is defined as the Cassie- Baxter state [10]. Since most of the current hydrophobic layers are fabricated from soft polymeric materials [12-15] or enriched to the non-wetting state by applying a thin chemical modification layer, they are rarely resistant in harsh environmental conditions. This point led researchers to demand the hydrophobicity in intrinsically hydrophobic hard metals [16-19].

In order to reach the desired morphologies, various fabrication methods are used including sol-gel, sputtering, physical and chemical vapor deposition, and electrodeposition [20-33]. In the field of the deposition of metals on conductive substrates, the one-step electrodeposition has more advantages as well as simplicity and cost-effectiveness than the rest of methods. This method is used in the fabrication of large scale in smart coating technologies. Since the morphology of a prepared surface by electrodeposition method is highly affected by variation of the applied current and voltage, various stimuli are definable. Herein, we have used the galvanostatic and cyclic voltammetry approaches in various bath temperatures. The galvanostatic deposition with the fixed current density and semi-constant voltage does not face any saturation or jumping in the I-V curve. So, fabrication of the distinct metal crystals is desirable due to the low deposition rate. However, it is desired to see the saturation states and spikes in the I-V curve in the cyclic voltammetry approach because of the possibility of reaching the higher current densities. It can be attributed to the change in analytics concentration near the working electrode compared to the bulk solution ones, due to the adsorption and desorption of ions to the substrate [28,30]. These huge changes could form a well-featured compact morphology.

In addition, it is well-known that bath temperature changes during the electrodeposition could affect the cathodic overpotential, viscosity of the solution, conductance of ions, and polarity of the electrodes [31- 41]. Therefore, both the nucleation and growth could be affected which consequently may change the morphology, grain refinement, coarsening, porosity, and compactness of the layer [31,41]. In fact, thermal energy affects the ions' mobility and their energy to overcome the potential barrier and form adatoms on the layer. Moreover, the larger current densities are reachable in the higher bath temperatures; hence, the influence of raising up the bath temperature is the decrease in the nucleation rate, as well as an increase in the crystal growth and formation of the larger crystals and thicker layers. In addition, it is observed that bath temperature has a reversible influence on the surface overpotential. This indicates bath

temperature influence is related to the kinetics of the growth process without changing in the electrical properties of the materials [42].

On the other hand, in the copper oxides the ratio between the Cu and oxygen is a key parameter which governs the surface energy of the sample. It is observed that surface energy would be decreased by lowering the oxygen amount of the outer layer while the overall chemical composition of the film remains unchanged [43]. It is difficult to detect these changes using the ordinary chemical composition characterization methods (XPS, FTIR, PL, and etc.) because the penetration depth of such methods is much larger than the surface atomic layers as well as the binding energy of copper and different copper oxides (Cu_xO), which are overlapped [44,45]. From the crystal structure view, the work function of a set of crystalline plates is increased by increasing its packing factor, which results a lower surface energy. Hence, in the cubic Cu_2O crystal, the {111} plates have the lowest surface energy and consequently the largest hydrophobicity [46]. Moreover, in the electrodeposition approach, the Cu_2O micrometric crystals may be grown in the shape of cubes, octahedral pyramids, triangles, and their truncated structures as well as dendrite structures and fractals [27-42, 47-49].

Herein, the copper oxide layers were grown on the gold/Si substrates using the galvanostatic and cyclic voltammetry approaches of the electrodeposition method to study the wetting transitions in different bath temperatures. Finally, the prepared samples were characterized using the atomic force microscopy (AFM), scanning electron microscopy (SEM), field emission scanning electron microscope (FE-SEM), energy dispersive X-ray (EDX), X-ray diffraction (XRD), optical profilometry, and contact angle goniometry.

2. Experimental details

2.1 Electrodeposition conditions

In this work, the galvanostatic and cyclic voltammetry, two different approaches of the electrodeposition method, were used to coat copper oxide layer on the gold/Si(100) substrates (θ_w=85°) at various bath temperatures. In order to change the bath temperature, the electrolyte container was put in a hot water bath at approximately constant temperatures of 15, 22, 30, 45, 60, 75, and 90°C during the deposition. The used electrolyte was a 0.1 M aqueous copper sulfate (Sigma Aldrich) solution with pH=4.68. The electrochemical experiments were performed with an Autolab potentiostat of Metrohm in both galvanostatic and cyclic voltammetry methods, as already reported [29]. A three-electrode system was connected to the potentiostat: a 150 nm gold on Si(100) wafer as a working electrode, a carbon rod as a counter-electrode and a saturated calomel electrode (SCE) as reference. In the galvanostatic method a constant current density 1 $\frac{mA}{cm^2}$ was used. In addition, the cyclic voltammetry deposition was performed using a fixed negative potential between -0.5 and -0.4 V as a working potential, 0.2 V higher than the corresponding oxidation potential at desired temperatures, with a fixed 0 V as a positive potential at a scan rate of 20 mV s^{-1} for 1 to 7 numbers of deposition cycles. After the electrodeposition, the samples were washed in distilled water and dried for one week at ambient conditions before the characterization.

2.2 Surface characterization

The θ_w and θ_{SA} were measured using a DSA30 goniometer (Krüss) with a 2 to 5 µL water droplet (γ_{LV} = 72.8 mN/m) at five different positions of each sample. XRD patterns of the samples were measured by Philips XRD X'pert MPD diffractometer (Cu Kα radiation, 1.54 Å) with a step size of 0.02˚ and count time of 1 s per step in 2θ, ranging from 10° to 80° at grazing incidence mode. A 6700F microscope (JEOL) was used to obtain the SEM images. A Hitachi S4160 FE-SEM and its connected Bruker XFlash 6L10 EDX system, were used to prepare SEM cross-sectional image and EDX data. Furthermore, an NT–MDT non-contact AFM (window size: 1-10 µm) was used to study the surface features more precisely. The average roughness was determined using a Wyko NT 1100 optical microscope (Bruker) with High Mag. Phase Shift Interference (PSI), the field of view 0.5X and objective 50X.

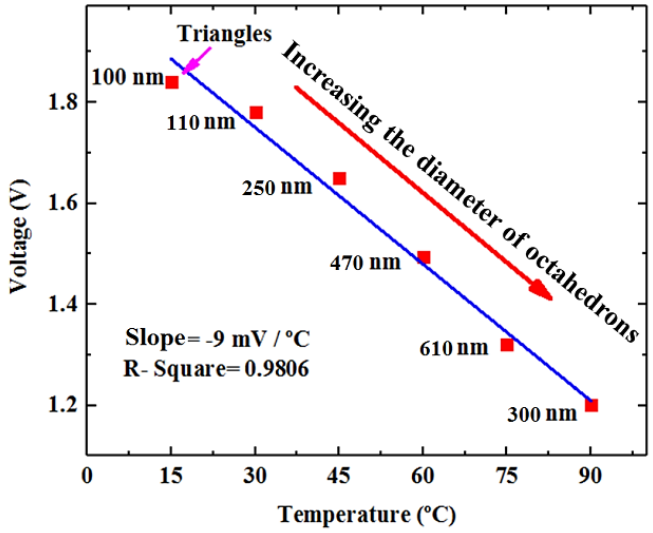

Figure 1: Changes in the working potential and the corresponding shape and size of the formed crystals on the surface by increasing the bath temperature.

3. Results

3.1 Galvanostatic deposition

The galvanostatic deposition method was used at different bath temperatures of 15, 30, 45, 60, 75, and 90 °C. All depositions were applied at a constant current density 1 $\frac{mA}{cm^2}$. As shown in Fig. 1, increasing the bath temperature results a linear decrease of working potential from 2 to 1 V with a rate of 9 $\frac{mV}{°C}$. Moreover, most of the samples have shown a crystal structure including nanotriangles and octahedral pyramids (octahedrons) such that their sizes were increased by raising the temperature up to 75 °C (this point will be discussed in details in the following using surface spectroscopy images). Herein, it is tried to investigate the effect of the temperature on the activation energy. The activation energy is the energy needed for the excitation of the surface charge carriers, which are holes in the case of Cu_2O [42], to the valence state leading to a large crystal growth. This is explained via an Arrhenius plot, the neutral logarithm of the deposition potential versus the inverse of the bath temperature (Fig. 2). The related equation is as the following [42]:

$$V = A\, e^{-E_a/RT}\,, \qquad (1)$$

where V, E_a, R, and T are the working potential, activation energy, gas constant, and the bath temperature, respectively. The pre-exponential factor A depends on the entropy of activation and relative

motion of reacting particles, too [42]. By fitting Eq. 1 to the more linear part of the measured data as plotted in Fig. 2, the calculated E_a is as small as6 $\frac{KJ}{mol}$ or 63 meV which is around 10 times smaller than the other reports in the galvanostatic deposition of copper [42]. It makes the deposition easier and increases the rate. Regarding the curves represented in Figs. 1 and 2, the overpotential is decreased gradually by increasing the temperature. It means that the formation of the large crystals in higher temperatures is desirable due to the huge rate of thermal excitation of charge carriers to the valence states and consequently increasing the crystal growth [42].

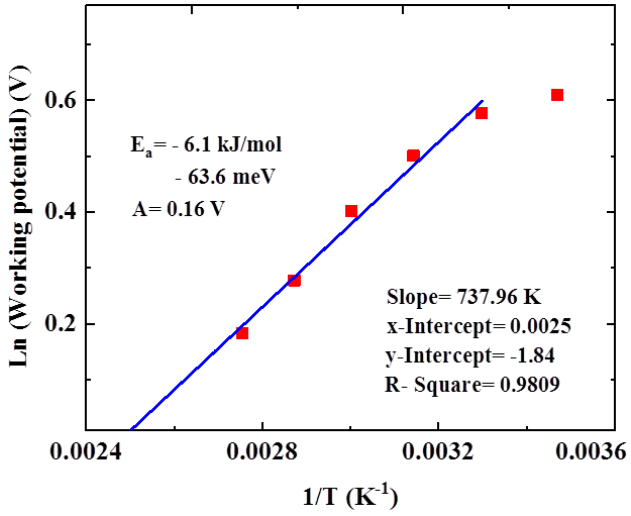

Figure 2: Logarithmic diagram of the working potential versus inverse temperature at a fixed current density ($1\ ^{mA}/_{cm^2}$).

The overall morphology of surfaces was studied by SEM images in Fig. SI1 (see Supporting Information). As it was previously reported by authors of [29], nano-triangles with approximately 100 nm in diameter are formed at 15 °C representing the growth along the Cu_2O (111) facets. Increasing the bath temperature to 30 °C leads to conversion of the surface crystals to the octahedral pyramids, depicting formation of (111) facets of the cubic Cu_2O crystals in another illustration. This manner of the surface structure growth was remained by increasing the bath temperature up to 75 °C.

Indeed, these octahedrons were enlarged by increasing the temperature and had an average diameter of 110, 250, 470, and 610 nm as well as 45, 135, 370, and 550 nm height at 30, 45, 60, and 75 °C, respectively (Fig. SI2). However, no specific morphology was observed at 90 °C, which indicates the low and non-epitaxial deposition of copper compounds at this temperature. AFM images of the prepared samples in 2 µm windows, shown in Fig. 3, support the crystallite morphology and measurement of the statistical data of each grown structure; thereby, by comparing the AFM and SEM images, it could be deduced that the contact surface of the octahedrons with the substrate is reduced by increasing the bath temperature to higher than 15°C, increasing the swelling factor of the crystallites (Fig. 4). According to the inset crystal shape in the figure, ratio of the half of larger diameter to the smaller ones in the octahedron formed from the intersection of {111} planes is equal to 0.707 (= $^{1}/_{\sqrt{2}}$). So, resulting from the Thales's theorem, the defined swelling factor used here is the ratio of the crystal height to the half of the largest diameter of the formed octahedron on the surface. It should be mentioned, when the swelling is larger than 100%, this definition of swelling makes an overestimation because the AFM analysis could not correctly represent the lower half of the crystal.

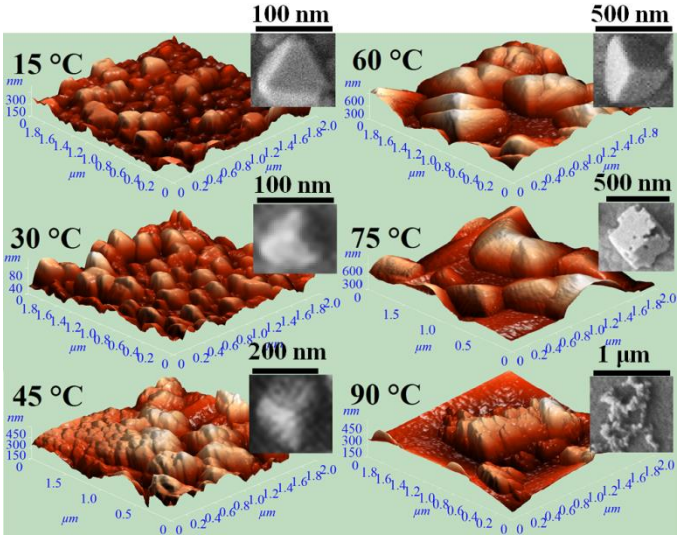

Figure 3: AFM images of the prepared samples in various bath temperatures using the galvanostatic method. In addition, an enlarged picture (inset) of grown crystal from the SEM (Fig. SI1) was applied to each image.

The variation in roughness of the prepared samples at various bath temperatures was shown in Fig. SI3. Accordingly, the roughness is increased by increasing the deposition time in almost all the bath temperatures, in agreement with the previous reports [27,35].

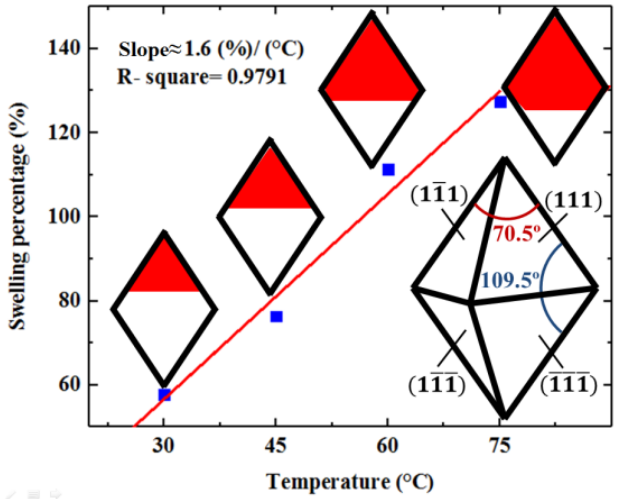

Figure 4: The swelling percentage of octahedral structures prepared at various bath temperatures and the corresponding schematic images. Moreover, a schematic illustration of various {111} planes of the cubic crystal and plane intersection angles were shown too.

However, the 90 °C sample is expected to have a small amount of copper deposition on the substrate. Moreover, the larger roughness was observed for samples at 15, 45, and 60 °C compared to the other samples. Still, the roughness of the layer was decreased by increasing the temperature to above 45 °C. These heterogeneous changes in the roughness due to the variation of bath temperature can be attributed to the major changes in morphology, which was investigated former with microscopic images.

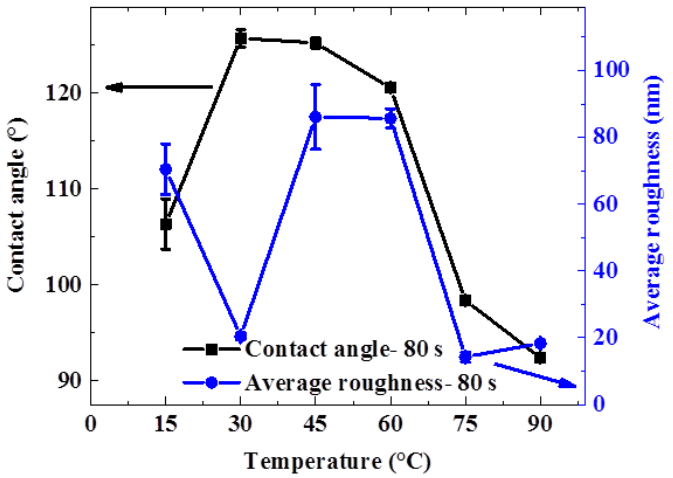

Figure 5: Comparative curves of contact angle and roughness of the prepared galvanostatic samples in various bath temperatures.

Hydrophobic behavior was observed for the prepared layers at various bath temperatures by measuring the contact angle of the water droplets on the samples (Fig. SI4). However, it is difficult to find a consistent trend for the contact angle at different bath temperatures. The maximum contact angle is observed in 80 s deposition samples for 30, 45, and 60 °C bath temperatures. For a better comparison, the contact angle and roughness curves of the samples prepared with 80 s deposition time were plotted against bath temperature as shown in Fig. 5. Similar behavior is observed for the roughness and contact angle of the samples except 30 °C sample. Again, the maximum contact angle of 135 ° is obtained for the 30 °C sample, where octahedrons made a good coverage on the surface. This sample showed a low roughness, too. Moreover, the contact angle dropped down sharply above 45 °C.

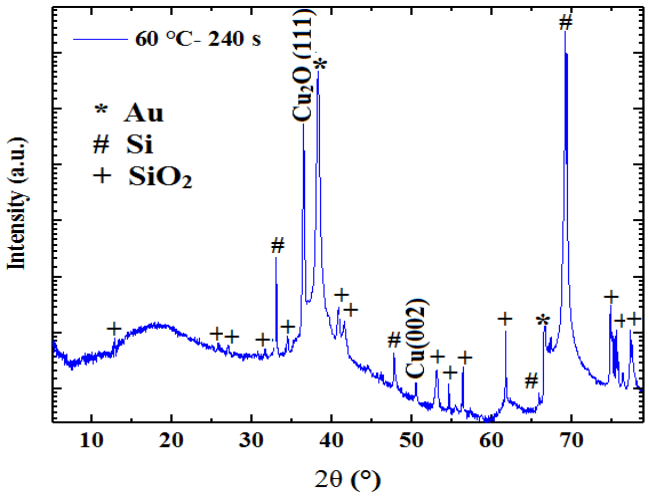

Figure 6: XRD pattern of the prepared sample at 60 °C with 240 s deposition time. The semi-epitaxial growth of structure on the (111) direction of Cu_2O cubic structure is obvious. Starred peaks are gold, silicon, and silicon oxide peaks.

The fabricated layer composition of the samples was studied using the resulted patterns from XRD characterization. A large Cu_2O (111) and a negligible Cu (002) peak was observed in the patterns (Fig. SI5). The Cu_2O (111) peak is approximately increased by increasing the temperature to 60 °C. However, it is very weak in 75 °C due to the distinct and low deposition of crystals in this temperature.

One of XRD patterns of the prepared samples, corresponding to 60 °C sample with 240 s deposition time, is shown in Fig. 6 to emphasize the existence of the Cu_2O (111) facets on the surface, which is in agreement with the formation of the octahedron pyramids in the SEM and AFM images. Based on our obtained results in the previous work [29], only the enough large peaks in the XRD patterns of galvanostatic samples prepared on Au/Si wafer substrates can be observed due to the thin and discontinuous layer as well as the strong XRD peaks of the substrate. Therefore, it is difficult to compare the height of the desired XRD peaks of the prepared layer by the galvanostatic method in the various fabrication conditions. The EDX analysis has shown the Cu/O ratio in these samples is in the range of 1.5 to 2.1 in the samples prepared at 15 to 60 °C (Fig. SI6). Therefore, the maximum amount of copper is formed at 60 °C. The Cu/O ratio is slightly larger than 2 in this temperature.

3.2 Cyclic voltammetry

In this method, various deposition temperatures including 15, 22, 30, 45, 60, and 75 °C were applied to the deposition system. Cathodic part of the voltammetry curve of the electrodeposition cell is shown in the Fig. SI7. Accordingly, the reduction to Cu_2O occurs at voltages in the range of -0.54 to -0.64 V at various bath temperatures. Regarding to the plateau of the I-V curves, although the cathodic current has not changed significantly during the increase of the bath temperatures from 15 to 60 °C (Fig. SI8), a sharp increase in the cathodic current density is observed at 75 °C, results in a sharp increase in the layer thickness (Fig. SI9). This effect indicates an improvement in the deposition rate at this temperature. On the other hand, according to voltage of the plateau, although the overall trend in the bath temperatures from 15 to 60 °C is to slightly decrease the amount of cathode voltage with temperature, there is an increase in the amount of voltage at 45 °C, which produces more irregular crystals in galvanostatic method as well as the formation of dendrite structures with fine particles in cyclic voltammetry method. This effect is in agreement with the literature [48 and 49].

The SEM images of the as-prepared samples have been shown in Fig. 7. It includes the images of the 3-scan samples made at 15, and 30 to 75 °C, as well as images of the 5-scan sample at 22 °C. The distinction in the proposed images of the 22 °C sample is to show the morphology of the most hydrophobic sample prepared in this work. Similar octahedral crystallite microstructures are observed for all the samples except that of 45 °C, which is partially covered with smaller particles. The orientation of flat facets of these structures in each image is almost identical. These facets have appeared in the shape of triangles, trapezoids, rhombus, and squares. The size of the micrometric structures on these surfaces is increased from 1 micrometer to 6 micrometers by raising up the bath temperature as listed in Table 1. In addition, average thickness of the layers is approximately increased by increasing the bath temperature, where thickness of the 75 °C sample is significantly larger than other ones (Fig. SI9). Moreover, these micrometric crystals are more prominent and cubic in the shape among the rest of samples for the case of 5-scan samples at 22 ° C. The existence of deep valleys on the surface made this sample more potent to be more hydrophobic than the other as-prepared samples; the wetting properties will be discussed in the following. According to Fig. 7 and Table 1, microcrystals in 15 °C

sample are more homogenous in size and smaller than those of the other samples except the 45 °C sample. As the temperature rises, the size of the crystals are increased where this crystalline size increase is faster in 60 and 75 °C, reaching to 6 micrometers. In addition, the crystallites in the 75 °C sample have more distortion and size fluctuation than the rest of samples. However, dendrite fractals in 45 °C samples are formed by repeating and interconnecting around 100 nm quadrilateral cubic structures such that there are cubic crystals as large as 500 nm on the tip or at the base of some fractal branches. Therefore, these rough porous and powdery structures allow the water droplet to penetrate and stick to the surface, decreasing the hydrophobicity.

Table 1: Table of crystal sizes of the prepared structures at various temperatures using cyclic voltammetry method.

Bath temperature (°C)	**15**	**22**	**30**	**60**	**75**
Crystallite size (µm)	1-1.2	1-3	1-2.7	4-5.5	2-6

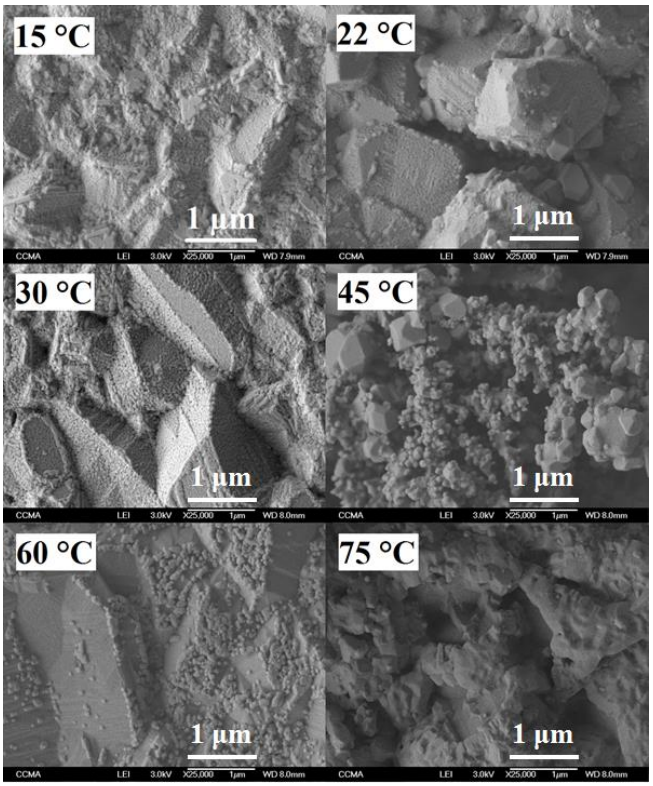

Figure 7: SEM images of the prepared samples at various bath temperatures using cyclic voltammetry method.

In general, investigating the XRD pattern of the samples (Fig. SI10) shows that the peaks of the layers are more numerous and more intense compared to those in the galvanostatic samples (Table 2). Observed peaks of the prepared layers belong to the copper and its oxides in various orientations. With the exception of the 45 °C sample, the largest peak in all samples is corresponding to Cu (002) planes, which indicates that the voltage balance of the system during the deposition is more suitable for the growth of copper than its oxides, in contrast with the galvanostatic method. Of course, it is desired due to the fact that the working potential of cyclic voltammetry was approximately 0.2 volt less than the oxidation potential of the system, does not allow the electrolyte to be oxidized effectively. However, though the largest peak in the 45 ° C sample is corresponding to the Cu_2O (111), the copper main peak is large enough, too. The resulted EDX data of the cyclic voltammetry samples shows that these layers are almost pure copper with very low amount of oxygen (Fig. SI11). Although, the change in the Cu/O ratio with the bath temperature is large but it maybe is a result of the low separability of the EDX data in small amounts of light materials (e.g.: oxygen).

Figure SI12 shows the roughness of the samples versus the number of deposition cycles at various bath temperatures. According to our latest work done on the electrodeposition of copper-based thin films [29], it is expected that the roughness of cyclic voltammetry samples is several times larger than the galvanostatic one. It can also be observed that the roughness is increased by increasing the number of deposition cycles which is more pronounced in 45 and 75 °C samples. The roughness remains almost constant for more than one deposition cycle in 15, 30, and 60 °C samples, which is raised 5, 20 and 40 times in 22, 75, and 45 °C, respectively. In addition, the roughness of 3 to 7 numbers of deposition cycles in 45 and 75 °C is at least 10 times larger than the similar samples in other bath temperatures which indicate a huge change in their surface structure.

Table 2: The relative intensity (corresponding to the largest XRD peak of the substrate (Au (111))) of the observed XRD peaks of the cyclic voltammetry samples at various temperatures.

Materials	**Peak positions (2θ) (°)**	**15 °C**	**22 °C**	**30 °C**	**45 °C**	**60° C**	**75 °C**
CuO (110)	**32.56**	-	0.14	-	-	-	-
Cu_2O (111)	**36.52**	0.25	0.03	0.2	**2.55**	0.1	**1.34**
Cu_2O (002)	**42.42**	-	-	-	0.23	-	0.24
CuO (-112)	**46.32**	0.08	0.04	0.04	0.06	0.23	0.24
Cu (002)	**50.45**	**0.82**	**2.38**	**1.01**	**1.44**	**1.6**	**6.47**
Cu (022)	**61.55**	0.08	0.12	0.13	0.11	0.08	0.19

According the contact angle curves in Fig. SI13, while the contact angle of the droplet in 22 °C sample is increased linearly by adding the number of deposition cycles, it is almost constant in 30 °C and decreased in 15 and 45 °C. This decrease is more intensive in 45 °C, where the wetting reached to superhydrophilicity in 7 numbers of deposition cycles. Consequently, although the smooth surface of 45 °C sample (with 1 cycle of deposition) is hydrophobic ($\theta_W > 90°$), the increase of roughness in samples with more than 1 cycle of deposition not only does not increase their hydrophobicity but also makes them superhydrophilic. This behavior indicates the Wenzel equation may is not enough to study these samples. Additionally, the powdery nature of the as-prepared samples causes distribution of the water in the layer. On the other hand, variation of the contact angle and roughness, caused by changing of the thickness of 22 °C samples, are similar. Hence, by increasing the number of deposition cycles, the roughness and contact angle are increased leading to the largest θ_W among the rest of samples in this work. However, despite a large enough θ_W, the water droplet adhered to the surface and did not drop down. It indicates that though the structure is able to trap air pockets and increase the water droplet contact angle, still the surface energy or the amount of air pockets are not enough to maintain the Cassie-Baxter [10] equation conditions to reach the superhydrophobicity. These samples are called parahydrophobic [9].

Eventually, according to the above discussion, the θ_W and roughness changes of the prepared samples at 3 numbers of deposition cycles are plotted versus bath temperature in Fig. 8. According to these curves, although it is difficult to find a uniform

behavior for the contact angle and roughness with temperature, it can be concluded that these parameters change against each other: when the roughness was increased by raising the bath temperature to 45 °C, the contact angle was increased at first and then decreased intensely to 105 °. So, the least hydrophobicity occurs in the largest roughness. At bath temperatures above 45 °C, the contact angle is increased linearly to reach 147 °, where the roughness has some fluctuations. These non-uniform changes in the contact angle and roughness are arising from the huge changes in the surface structure during the bath temperature variation, which was discussed in the SEM results.

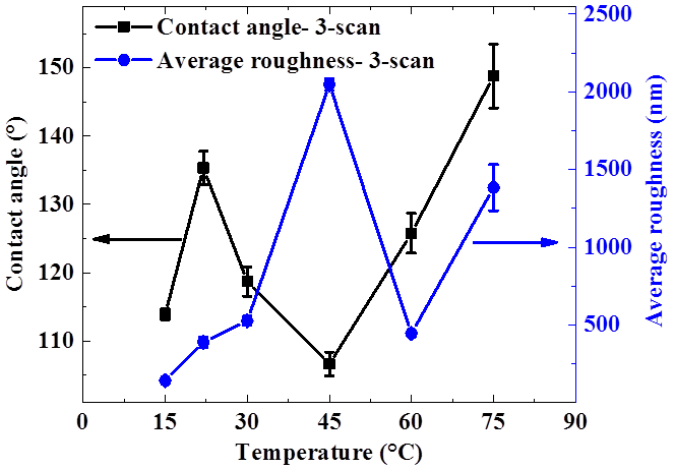

Figure 8: Comparison between changes in the contact angle and roughness of the prepared cyclic voltammetry samples at various bath temperatures with 3 numbers of deposition cycles.

3.3 Improvement of the samples hydrophobicity by the rest time

Characterizing wetting of the stored samples in a sealed glass box for a long period of time (more than one year), it was observed that although all samples have been gotten more hydrophobic by time, this change is more in the prepared sample at 45 °C using cyclic voltammetry method for three numbers of scans. In this sample, the θ_W is increased from 107 º at the as-prepared sample to 151 º with θ_{SA} smaller than 36º. It can be dedicated to the conversion of the layer from powdery to the perfect sticky one by a long term rest (this sample is not powdery anymore). Moreover, a complex fractal structure formed from the interconnection of different sized nanometer quadrilateral cubes maintains enough surface exposure to the air which results in more change in the surface chemical composition than the other samples. According the previous reports and observations [44,45], the decrease in oxygen amount of the surface layer is effective in this huge change of wetting. In addition, the prepared sample at 75 °C with 3 numbers of scans in the cyclic voltammetry method is converted from parahydrophobic to superhydrophobic with θ_{SA} smaller than 3º. Finally, it should be mentioned that the larger change in the hydrophobicity with the rest time happens in the roughest surfaces (45 and 75 °C cyclic voltammetry samples).

4. Discussion

According to the above results, the diameter and swelling of the formed triangle and octahedral crystals at samples were increased almost linearly by raising the bath temperature. Moreover, the flat facets in both structures are corresponding to the (111) direction of Cu_2O which is confirmed by the XRD patterns. In addition, the working potential of the galvanostatic deposition is decreased linearly by increasing the bath temperature with activation energy as low as –0.063 eV resulting in a less over-potential. One consequence of this fast change is the overcoming of crystal growth to the nucleation during deposition and consequently the formation of larger crystals in the higher temperatures. Furthermore, this activation energy is 10 times smaller than the other reports on the galvanostatic deposition of copper in various bath temperatures (which are about 0.6 to 0.8 eV) [42]. However, the deposition rate at 90 °C is low due to the huge increase of the thermal ion fluctuations near the boiling point of the solvent (ultra-pure water). In fact, it is difficult to attribute a special trend to the dependence of roughness to the temperature of the galvanostatic samples because height, diameter, and coverage of the surfaces are changed variously. However, trend of the roughness and contact angle at a fixed deposition time are similar, except at 30 °C. This distinct sample supports a smooth surface with good coverage providing convenient conditions to develop Cassie- Baxter state [10].

On the other hand, most of the prepared samples by the cyclic voltammetry method represent large octahedral crystals (with diameters from 1 to 6 µm by raising the bath temperature) with flat facets except for the prepared samples at 45 °C which had a semi-dendrite structure. Moreover, the morphologies at 22 °C are more cubic with deep and narrow valleys between the structures resulting in a large contact angle, 148 °. However, the formed structures at 45 °C are semi-fractal structures with many long branches that have 500 nm cubes on the tip or at the base of branches. The fingerprint of the morphology difference between the sample at 45 °C and the others is also obvious in their XRD patterns. These patterns show the formation of Cu (002) crystals on the surface of all the samples except for the sample 45 °C. Nonetheless, there is a Cu_2O (111) peak in the 45 °C sample larger than the Cu one. In comparison with the galvanostatic samples, the optical roughness of cyclic voltammetry samples and its changes with bath temperature are significantly large (up to 40 times). The water contact angle on cyclic voltammetry samples raised up to 147 ° in 75 °C with adhesion to the surface which is called a parahydrophobic phase. Hence, in comparison with the galvanostatic samples, increasing the Cu/O ratio may increase the hydrophobicity as well as the surface coverage. It should also be emphasized that the hydrophobicity of all the samples were increased by the rest for a long time where the highest raise happened in the prepared sample at 45 °C (θ_W changes from 107 ° to 151 °) as it was not powdery anymore. In addition, since the fractal structure may provide the more accessible surface to the air, more modification in the chemical composition of the outer layers is desirable. Finally, the cyclic voltammetry sample prepared at 75 °C was converted from parahydrophobic to superhydrophobic with $\theta_{SA} < 3$ º after a long time rest in the sealed glass box.

5. Conclusions

In summary, copper and cuprite layers were fabricated on gold/Si substrates using the galvanostatic and cyclic voltammetry approaches of electrodeposition method at various bath temperatures ranging from 15 to 90 °C. However, the deposition at 90 °C and higher temperatures is almost impossible due to the high thermal fluctuations of ions and their disruptive effect on the mobility of the ions. It was observed that in the galvanostatic deposition, distinct and

well-defined cuprite crystals in the shape of triangles and octahedrons were formed. The size of crystals and their swelling from the surface were increased by increasing the bath temperature. On the other hand, compact morphology with large micrometric crystals (1 to 6 µm in diameter) was grown in the cyclic voltammetry method, except in 45 ºC where a powdery semi-fractal structure was formed. In this work, highest hydrophobicity of the as-prepared samples happened in the prepared samples at 75 ºC by cyclic voltammetry method (θ_W = 147º, parahydrophobic). By long term rest in a sealed glass box, wetting of the samples was converted from the hydrophilic to parahydrophobic (θ_W = 151º) in the as-prepared sample at 45 ºC by cyclic voltammetry method. In addition, the parahydrophobic 75 ºC sample changed to superhydrophobic by the θ_{SA} < 3 º. It is expected that this one-step deposition and the resulted in superhydrophobicity without any secondary chemical modification could find convenient applications in the fabrication of smart surfaces in different industries.

Acknowledgments

Partial financial support from the Research Council of the University of Tehran and Iranian National Science Foundation under grant # 95849613 is acknowledged. The authors also thank Iran nanotechnology initiative council and the Centre Commun de Microscopie Appliquée (CCMA), Nice, France, for the SEM images.

References

[1] T. Darmanin and F. Guittard, Bioinspired Superhydrophobic Surfaces: Advances and Applications with Metallic and Inorganic Materials (Pan, Stanford, USA, 2017).
[2] Y. Si and Z. Guo, Nanoscale 7 (2015) 5922–5946.
[3] J. Liu, X. Huang, Y. Li, Z. Li, Q. Chi and G. Li, Solid State Sci. 10 (2008) 1568–1576.
[4] P. Zhang and F.Y. Lv, Energy 82 (2015) 1068–1087.
[5] Z. Xue, Y. Cao, N. Liu, L. Feng and L. Jiang, J. Mater. Chem. A 2 (2014) 2445- 2460.
[6] G. Zhu, Y. Su, P. Bai, J. Chen, Q. Jing, W. Yang and Z. L. Wang, ACS Nano 8 (2014) 6031- 6037.
[7] K. K. Varanasi, T. Deng, J. D. Smith, M. Hsu and N. Bhate, Appl. Phys. Lett. 97 (2010) 234102- 234104.
[8] T. Darmanin and F. Guittard, J. Mater. Chem. A 2 (2014) 16319-16359.
[9] A. Marmur, Soft Matter 8 (2012) 6867- 6870.
[10] A. B. D. Cassie and S. Baxter, Trans. Faraday Soc. 40 (1944) 546–551.
[11] R. N. Wenzel, Ind. Eng. Chem. 28 (1936) 988–994.
[12] G. R. Chagas, R. Akbari, G. Godeau, M. R. Mohammadizadeh, F. Guittard and T. Darmanin, ChemPlusChem 82 (2017) 1351– 1358.
[13] J. J. Victor, D. Facchini and U. Erb, J. Mater. Sci. 47 (2012) 3690- 3697.
[14] T. Darmanin and F. Guittard, J. Am. Chem. Soc. 133 (2011) 15627–15634.
[15] T. Darmanin, E. Taffin de Givenchy, S. Amigoni and F. Guittard, Adv. Mater. 25 (2013) 1378- 1394.
[16] G. Azimi, R. Dhiman, H.-M. Kwon, A. T. Paxson and K. K. Varanasi, Nat. Mater. 12 (2013) 315- 320.
[17] L. Martínez, E. Román, J. L. De Segovia, S. Poupard, J. Creus and F. Pedraza, Appl. Surf. Sci. 257 (2011) 6202- 6207.
[18] K. Jiang, Fabrication and Catalytic Property of Cerium Oxide Nanomaterials (University of Nebraska-Lincoln, Lincoln, USA, 2011).
[19] J. Tam, B. Feng, Y. Ikuhara, H. Ohta, and U. Erb, Adv. Mater. Interfaces 1700850 (2017) 1-11.
[20] J. Li, Y. Long, C. Xu, H. Tian, Y. Wu and F. Zha, Appl. Surf. Sci. 433 (2018) 374–380.
[21] J. Song, S. Huang, Y. Lu, X. Bu, J. E. Mates, A. Ghosh, R. Ganguly, C. J. Carmalt, I. P. Parkin, W. Xu and C. M Megaridis, ACS Appl. Mater. Interfaces 6 (2014) 19858–19865.
[22] R. Jain and R. Pitchumani, Langmuir 34 (2018) 3159–3169.
[23] T. Aytug, D. F Bogorin, P. M Paranthaman, J. E Mathis, J. T Simpson and D. K Christen, Nanotechnology 25 (2014) 245601-245607.
[24] L. kong, X. H. Chen, L. G. Yu, Z. S. Wu and P. Y. Zhang, ACS Appl. Mater. Interfaces 7 (2015) 2616–2625.
[25] A. Eskandari, P. Sangpour and M.R. Vaezi, Mater. Chem. Phys. 147 (2014) 1204–1209.
[26] I. A. Hassan, I. P. Parkin, S. P. Nair and C. J. Carmalt, J. Mater. Chem. B 2 (2014) 2855–2860.
[27] S. Bijani, L. Martinez, M. Gabas, E. A. Dalchiele and J.-R. Ramos-Barrado, J. Phys. Chem. C 113 (2009) 19482–19487.
[28] M. Schlesinger and M. Paunovic (Editors), Modern Electroplating, Chapter 2: Electrodeposition of Copper, 5th Edition (JohnWiley&Sons, New Jersey, USA, 2010).
[29] R. Akbari, G. Ramos Chagas, G. Godeau, M. R. Mohammadizadeh, F. Guittard and T. Darmanin, Appl. Surf. Sci. 443 (2018) 191-197.
[30] A. J. Bard and L. R. Faulkner, Electrochemical Methods-Fundamentals and Applications, 2nd Edition (JohnWiley&Sons, New Jersey, USA, 2000).
[31] H. Natter and R. Hempelmann, J. Phys. Chem. 100 (1996) 19525-19532.
[32] M. C. Huang, T. Wang, W. S. Chang, J. C. Lin, C. C. Wu, I. C. Chen, K. C. Peng, S. W. Lee, Appl. Surf. Sci. 301 (2014) 369–377.
[33] X. Sui, Y. Huang, T. Han and X. Zeng, AIP Conf. Proc. 1829 (2017) 020042 (1-8).
[34] X. Zhang, Y. Zhang, H. Huang, J. Cai, K. Ding and S. Lin, New J. Chem. 42 (2017) 458-464.
[35] M. L. Free, R. Bhide, A. Rodchanarowan and N. Phadke, ECS Trans. 2 (2006) 335-343.
[36] S. C. Barnes, G. G. Storey and H. J. Pick, Electrochim. Acta 2 (1960) 195- 206.
[37] L. Cifuentes and J. Simpson, Chem Eng Sci. 60 (2005) 4915 – 4923.
[38] A. Mallik and B. Chandra Ray, J. Mater. Res. 16 (2013) 539-545.
[39] S. Z. El Abedin, A.Y. Saad, H.K. Farag, N. Borisenko, Q.X. Liu and F. Endres, Electrochim. Acta 52 (2007) 2746–2754.
[40] R. Akbari, G. Godeau, M.R. Mohammadizadeh, F. Guittard, T. Darmanin, ChemPlusChem 84 (2019) 368-373.
[41] A. Mallik and B. C. Ray, Int. J. Electrochem. Sci. 568023 (2011) 1-16.
[42] P. E. de Jongh, D. Vanmaekelbergh and J. J. Kelly, Chem. Mater. 11 (1999) 3512-3517.
[43] Y. Maimaiti, M. Nolan and S. D. Elliott, Phys. Chem. Chem. Phys. 16 (2014) 3036–3046.

[44] R. Akbari, M.R. Mohammadizadeh, M. Khajeh Aminian and M. Abbasnejad, Appl. Phys. A Mater. Sci. Process 125 (2019) 190-196.
[45] S. H. Tu, H. C. Wu, C. J. Wu, S. L. Cheng, Y. J. Sheng and H. K. Tsao, Appl. Surf. Sci. 316 (2014) 88–92.
[46] A. Soon, M. Todorova, B. Delley and C. Stampfl, Phys. Rev. B: Condens. Matter Mater. Phys. 75 (2007) 125420- 125429.
[47] M.J. Siegfried and K.S. Choi, J. Am. Chem. Soc. 128 (2006) 10356–10357.
[48] M.J. Siegfried and K.S. Choi, Angew. Chem. Int. Ed. 47 (2008) 368–37.
[49] M. J. Siegfried and K. S. Choi, Angew. Chem., 2005, 117, 3282–3287.
[50] Y. G. Lee, J. R. Wang, M. J. Chuang, D. W. Chen and K. H. Hou, Int. J. Electrochem. Sci., 2017, 12, 507 – 516.
[51] W. Zhao, W. Fu, H. Yang, C. Tian, M. Li, Y. Li, L. Zhang, Y. Sui, X. Zhou, H. Chen and G. Zou, CrystEngComm, 2011, 13, 2871-2877.